Journal of Catalysis **190,** 247–260 (2000)
doi:10.1006/jcat.1999.2780, available online at http://www.idealibrary.com on IDEAL®

# Influence of Ceria and Lanthana Promoters on the Kinetics of NO and $N_2O$ Reduction by CO over Alumina-Supported Palladium and Rhodium

Joseph H. Holles, Matthew A. Switzer, and Robert J. Davis[1]

*Department of Chemical Engineering, University of Virginia, Charlottesville, Virginia 22904-4741*

Received June 24, 1999; revised December 8, 1999; accepted December 8, 1999

**The kinetic parameters of the NO + CO and $N_2O$ + CO reactions over alumina-, ceria/alumina-, and lanthana/alumina-supported Rh and Pd were determined from 425 to 625 K. For NO + CO, the presence of ceria and lanthana affected activity, apparent activation energy, dinitrogen selectivity, and reaction orders to varying degrees over both Pd and Rh. The turnover frequency (based on $H_2$ chemisorption) for the ceria-promoted Pd catalyst was at least an order of magnitude greater than those for all other catalysts. Lanthana-promoted Pd was the next most active catalyst. Changes in kinetic parameters indicated that both ceria and lanthana facilitated NO dissociation on both Pd and Rh, but the effect of ceria on Pd was the most profound. For $N_2O$ + CO, ceria promoted the reaction rate on both Pd and Rh whereas lanthana did not promote the reaction on either metal. The ceria-promoted Pd catalyst was again the most active. However, the turnover frequencies for the $N_2O$ + CO reaction were about an order of magnitude lower than those for the NO + CO reaction under similar conditions. The rare earth components had very little effect on the activation energies and reaction orders for the $N_2O$ + CO reaction.** *In situ* **infrared spectroscopy showed the presence of isocyanate surface species on $Rh/Al_2O_3$ but not on $Pd/Al_2O_3$, which suggested two different reaction mechanisms for the $N_2O$ + CO reaction. No synergistic effect on $NO_x$ reduction was observed for a Pd/Rh bimetallic sample.** 

*Key Words:* **NO; $N_2O$; $NO_x$; CO; Pd (palladium); Rh (rhodium); lanthana; ceria; kinetics; reduction; NO + CO reaction; $N_2O$ + CO reaction; chemisorption.**

## INTRODUCTION

Automobile exhaust catalysts are designed to reduce emissions of carbon monoxide, nitrogen oxides, and uncombusted hydrocarbons. These catalysts typically contain noble metals such as Pt, Pd, and Rh. The principal function of the rhodium is to control emissions of nitrogen oxides (1). Removal of $NO_x$ is accomplished by reaction with carbon monoxide to form mostly dinitrogen and carbon dioxide, but previous studies of this reaction have reported the formation of nitrous oxide as a side product (2–4). Nitrous oxide can also undergo further reaction with carbon monoxide to produce the desired products dinitrogen and carbon dioxide (2, 5). The overall reaction scheme can be represented by the following three reactions:

$$CO + NO \rightarrow \frac{1}{2}N_2 + CO_2 \quad [1]$$

$$CO + 2NO \rightarrow N_2O + CO_2 \quad [2]$$

$$CO + N_2O \rightarrow N_2 + CO_2. \quad [3]$$

Alumina- and silica-supported rhodium catalysts have been thoroughly investigated as catalysts for $NO_x$ reduction (3, 4, 6, 7). The low-temperature activity of $Rh/Al_2O_3$ increased as the metal particle size increased, and the support was found to have little effect on selectivity (8). Ceria is added to automotive exhaust catalysts as a promoter and is postulated to enhance the water gas shift reaction and to function as an oxygen storage component (1). Ceria affects the NO + CO reaction on Rh by suppressing $N_2O$ formation, decreasing the apparent activation energy, and shifting the rate dependence on NO partial pressure to positive order (3). Since $N_2O$ can be an important side product, the $N_2O$ + CO reaction over Rh(111) single-crystal surface and alumina-supported rhodium particles has also been investigated (5, 9).

In addition to ceria, other rare earth oxides such as lanthana are added to the alumina washcoat of automotive catalysts for thermal stabilization (1). Lanthanum ions can also be incorporated directly into the ceria promoter to increase its oxygen storage capacity through extrinsic defects (10). Pure $La_2O_3$ catalyzes the NO + CO reaction under high-temperature conditions (11), but it is much less active than Rh for the reaction. Interestingly, rhodium supported on lanthana has been shown to have higher activity and apparent activation energy for the NO + CO reaction than Rh on alumina (7). In related work, Pd supported on lanthana has been examined as a catalyst for simulated engine exhausts (12, 13).

[1] To whom correspondence should be addressed. Fax: (804) 982-2658. E-mail: rjd4f@virginia.edu.



0021-9517/00 $35.00

The demand for additional rhodium in automotive exhaust catalysts to meet more stringent emissions controls for new automobiles accounts for a large portion of the Western-world consumption of rhodium (1). Palladium has been identified as one possible alternative for rhodium since it is more plentiful and has been found to be more durable at higher reaction temperatures (14, 15). As a result, the $NO + CO$ reaction has been studied over Pd single crystals (16, 17), planar model supported $Pd/Al_2O_3/Ta(110)$ catalysts, and high surface area $Pd/Al_2O_3$ powder catalysts (15, 18–20).

Typical three-way catalysts do not promote $NO_x$ reduction except in a narrow temperature window in the vicinity of catalyst lightoff (1). This is a concern during cold start since the catalyst has not yet warmed up to operating temperatures and a significant amount of total emissions are released during this period. Thus the present investigation examines the effect of ceria and lanthana on the kinetics of $NO_x$ reduction over rhodium and palladium catalysts in the relatively low temperature range of 425–625 K. The catalysts include $Pd/Al_2O_3$, $Rh/Al_2O_3$, $Pd/CeO_x/Al_2O_3$, $Pd/La_2O_3/Al_2O_3$, $Rh/CeO_x/Al_2O_3$, $Rh/La_2O_3/Al_2O_3$, and $Pd/Rh/Al_2O_3$. This approach allows the comparison of results between the different metals as a function of promoter.

## EXPERIMENTAL METHODS

The $Pd/Al_2O_3$ samples were prepared by slurrying $\gamma$-$Al_2O_3$ (Alfa Aesar, 99.97%) and palladium(II) acetylacetonate (acac) (Aldrich, 99%) in toluene for 2 h at 353 K and drying under vacuum in a rotary evaporator followed by 24 h in air at 473 K. Samples were then calcined in flowing air (BOC gases) by heating to 673 K at 0.5 K $min^{-1}$ and then remaining at 673 K for 4 h. Subsequent reduction of the catalyst occurred at 673 K for 2 h in flowing dihydrogen (99.999% from BOC gases, passed through a Matheson Model 8371V purifier). The $Rh/Al_2O_3$ samples were prepared in the same way using rhodium(III) acetylacetonate (Aldrich, 97%). The palladium/rhodium bimetallic catalyst was prepared using an appropriate mixture of Pd(acac) and Rh(acac). For catalysts supported on $CeO_x/Al_2O_3$ and $La_2O_3/Al_2O_3$, the promoter was first deposited on the alumina by slurrying cerium(III) acetylacetonate hydrate or lanthanum(III) acetylacetonate hydrate (Aldrich) and alumina in toluene for 2 h at 353 K and then drying and calcining as described above. The metal (palladium or rhodium) was then deposited on the $CeO_x/Al_2O_3$ or $La_2O_3/Al_2O_3$ using the same procedure as that used for the alumina-supported samples.

The reaction experiments were performed in a quartz reactor containing approximately 50 mg of catalyst diluted in chromatographic silica gel (Fisher) supported on a quartz frit. Feed gases included 5.00% NO/5.07% CO/He, $N_2O$ (99.97%), and He (99.999%) from BOC Gases, CO (UHP) from Air Products, and NO (99%) from MG Industries. Gas flow rates were controlled using mass flow controllers (Brooks Series 5850C) and varied from 5 to 250 ml $min^{-1}$. The total pressure in the reactor was near atmospheric, and partial pressures of the reactants were varied by changing the individual flow rates while simultaneously adjusting the flow rate of pure He. Reactant and product analyses involved a combination of gas chromatography (HP 5890 Series II with an Alltech CTR I column) and mass spectrometry (Dycor MA 100 model). The standard catalyst pretreatment consisted of heating at approximately 523 K for 1 h under flowing He. Product analysis was performed after a period of 45 min on stream under each set of reaction conditions to allow the reaction to reach steady state. Arrhenius plots were determined using 5.07 kPa each of NO and CO for the $NO + CO$ reaction and 4.05 kPa each of $N_2O$ and CO for the $N_2O + CO$ reaction. For the determination of reaction orders, the partial pressures of NO or CO, and $N_2O$ or CO, were held constant at 4.05 kPa while the pressure of the other gas was varied from 1.01 to 16.2 kPa.

The percentage of the metal atoms exposed was determined using $H_2$ chemisorption (99.999% from BOC gases through a Supelco OMI purifier) in a Coulter Omnisorp 100CX system. Adsorption isotherms were obtained at 303 K. The hydrogen uptake was calculated from the difference between total chemisorption and reversible chemisorption. Elemental analysis was performed by Galbraith Laboratories Inc, Knoxville, TN.

The FT-IR spectra were collected using a Bio-Rad FTS-60A in the transmission mode. The sample holder consisted of a stainless steel cylinder with KBr windows. Entrance and exit feedthroughs allowed for flow of gases through the cell. The temperature was monitored with a thermocouple placed in contact with a self-supporting sample pellet. Scans were recorded from 400–4000 wavenumbers with a resolution of 2 $cm^{-1}$. Samples were heated to 698 K in flowing dihydrogen to first reduce the metal and then cooled to 573 K in flowing helium. Scans were then recorded at 573 K with reactant gases flowing (5% $N_2O$ and 5% CO in He). After flow was halted, the cell was purged with helium, and scans were recorded. Finally, scans were obtained after evacuation of the cell to at least 10 mPa using a Pfeiffer TPU-260 turbomolecular vacuum pump.

## RESULTS

Results from elemental analysis are presented in Table 1. The loadings of rhodium were typically lower than those of palladium due to the geometric form of the precursor. The $Pd(acac)_2$ molecule is essentially planar which allows easy contact between the central Pd atom and the substrate. However, $Rh(acac)_3$ is three-dimensional and requires breakdown of the molecule during calcination before the Rh atom can efficiently contact the substrate (21). As

**TABLE 1**

**Elemental Analyses and Chemisorption Results**

| Catalyst | Wt% metal[a] | Wt% cerium or lanthanum | H/M[b] |
|---|---|---|---|
| $Pd/Al_2O_3$ | 4.92 | — | 0.18 |
| $Pd/CeO_x/Al_2O_3$ | 4.12 | 10.66 | 0.46 |
| $Pd/La_2O_3/Al_2O_3$ | 4.59 | 14.79 | 0.10 |
| $Rh/Al_2O_3$ | 1.85 | — | 0.40 |
| $Rh/CeO_x/Al_2O_3$ | 4.46 | 10.57 | 0.36 |
| $Rh/La_2O_3/Al_2O_3$ | 3.65 | 14.55 | 0.15 |
| $Pd/Rh/Al_2O_3$ | 1.85[c]/1.41[d] | — | 0.18 |

[a] Quantitative analysis by Galbraith Laboratories Inc.
[b] Total chemisorption–reversible chemisorption at 303 K.
[c] Weight percent palladium.
[d] Weight percent rhodium.

a result, an appreciable amount of $Rh(acac)_3$ was removed during the calcination process.

The loadings of cerium and lanthanum were on the order of that needed for a theoretical monolayer (~9 wt% Ce, based on the Ce surface density of 4.83 Ce/nm$^2$ derived from the $CeO_2$(110) plane and 26 wt% La from Ref. (22)). Very small and broad X-ray diffraction peaks associated with $CeO_2$ and $La_2O_3$ indicated that the promoters were well dispersed on the alumina.

Results from $H_2$ chemisorption on the supported metals are included in Table 1. The presence of ceria did not significantly affect Rh dispersion but more than doubled the Pd dispersion. Dihydrogen adsorption isotherms for $Rh/Al_2O_3$, $Pd/Al_2O_3$, and $Pd/Rh/Al_2O_3$ are presented in Figs. 1a–1c. The isotherms for $Rh/Al_2O_3$ are typical for chemisorption of dihydrogen on a metal particle. The isotherms for $Pd/Al_2O_3$ exhibit a large uptake of dihydrogen at about 3 kPa due to the formation of a $\beta$-phase hydride which is stable at 303 K at pressures greater than 2.3 kPa (23). The isotherms for $Pd/Rh/Al_2O_3$ do not show the large uptake associated with $\beta$-hydride formation in Pd particles. This result likely indicates that the $Pd/Rh/Al_2O_3$ catalyst contains bimetallic particles instead of separate particles of pure Rh and Pd on the support. Another possible explanation that we consider unlikely due to the catalyst synthesis conditions is that separate particles of Pd are too small to have significant internal volume to form the $\beta$-phase hydride.

For the NO + CO reaction, the only products observed were $N_2$, $N_2O$, and $CO_2$. No $NO_2$ was detected in any reaction run. For the $N_2O$ + CO reaction, the products

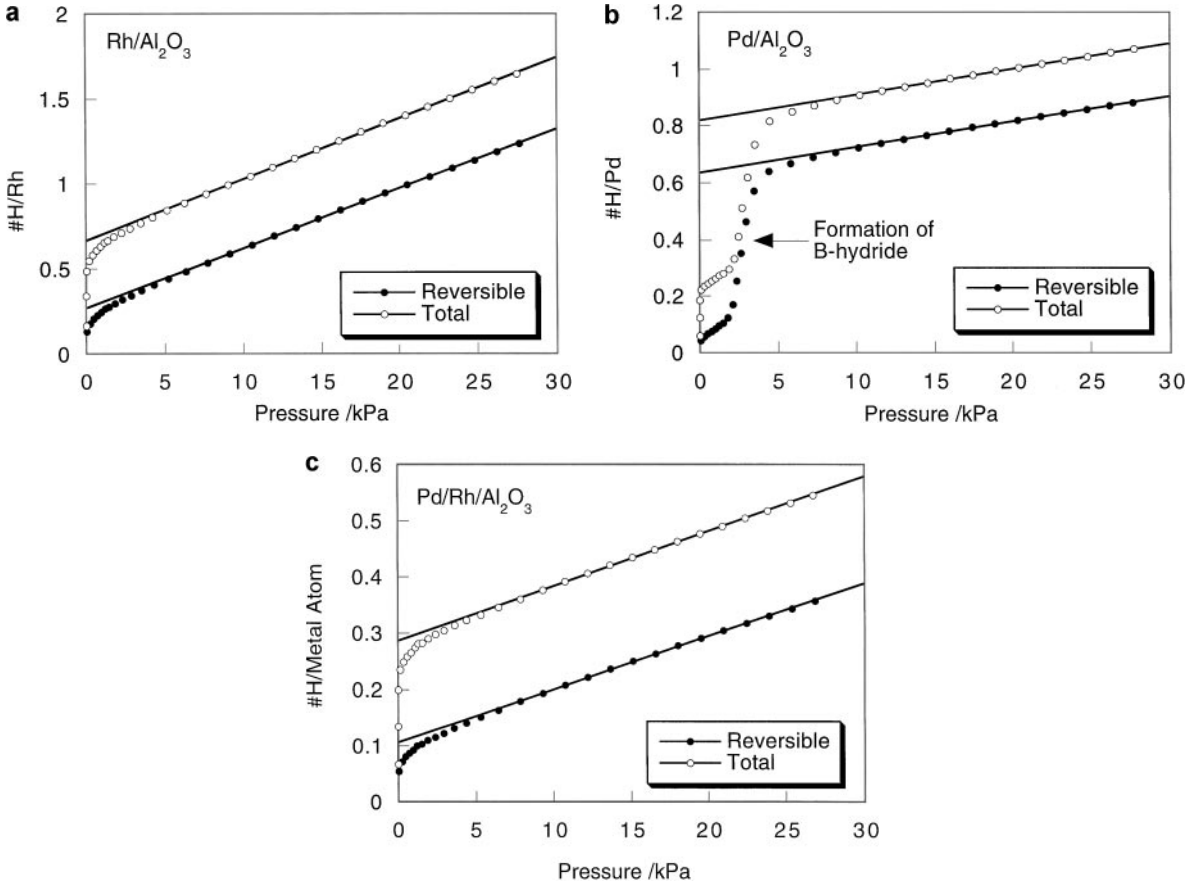


**FIG. 1.** Dihydrogen chemisorption isotherms for (a) $Rh/Al_2O_3$, (b) $Pd/Al_2O_3$, and (c) $Pd/Rh/Al_2O_3$. Lines indicate extrapolated values of total and reversible dihydrogen uptake.

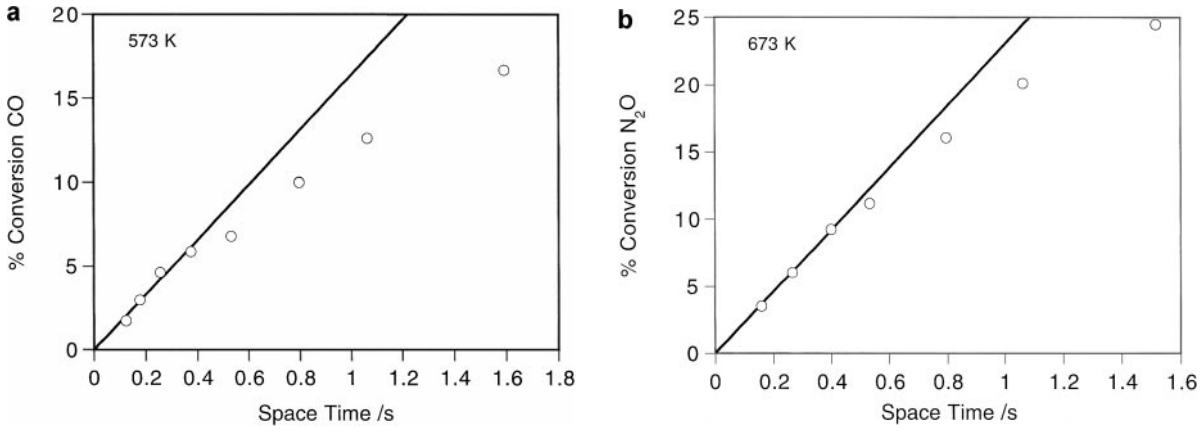


**FIG. 2.** Plot of conversion for the (a) NO + CO and (b) $N_2O$ + CO reactions as a function of space time (catalyst volume/volumetric flow rate) at 573 and 673 K, respectively, 4.05 kPa NO or $N_2O$, and 4.05 kPa CO for $Pd/CeO_x/Al_2O_3$. Typical conversion was 3–6% for all catalysts.

were $N_2$ and $CO_2$, and for the $N_2O$ decomposition reaction, the only products were $N_2$ and $O_2$. Figures 2a and 2b show CO conversion for the NO + CO reaction and $N_2O$ conversion for $N_2O$ + CO as a function of reactor space time (volume catalyst/volumetric flow rate) at 573 and 673 K, respectively, over $Pd/CeO_x/Al_2O_3$. Reactant flow rates were varied to change space time. Linear conversion (up to 6%) with space time indicates differential behavior and the absence of significant external transport effects on the measured rates. Evaluation of the Weisz–Prater criterion indicates that no pore diffusion limitations exist. Conversions for these experiments were kept in the 3–6% range.

Rates for the three different reactions (NO + CO, $N_2O$ + CO, and $N_2O$ decomposition) are compared in Fig. 3, which shows Arrhenius-type plots for each reaction over $Rh/Al_2O_3$. Comparing the curves at a common temperature of 553 K yields a ratio of turnover frequencies of 1 : 2.9 : 31.8 for the $N_2O$ + CO, $N_2O$ decomposition, and the NO + CO reactions, respectively. Figure 3 also shows that the three reactions have different apparent activation energies (109 kJ $mol^{-1}$ for the $N_2O$ + CO reaction, 139 kJ $mol^{-1}$ for the $N_2O$ decomposition reaction, and 86.6 kJ $mol^{-1}$ for the NO + CO reaction).

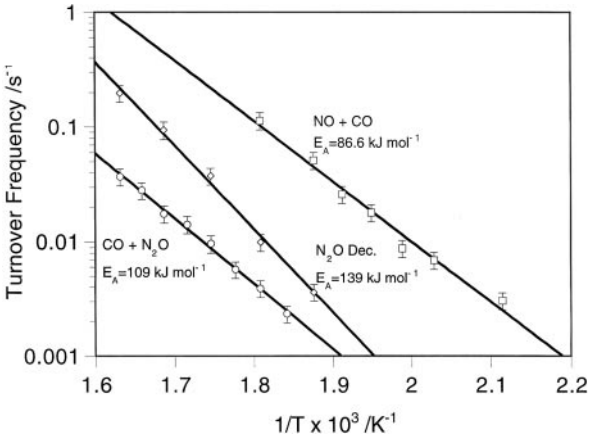


**FIG. 3.** Arrhenius-type plots for NO + CO, $N_2O$ + CO, and $N_2O$ decomposition reactions over $Rh/Al_2O_3$. Conditions were 5.07 kPa each of NO and CO for the CO + NO reaction, 4.05 kPa each of $N_2O$ and CO for the $N_2O$ + CO reaction, and 4.05 kPa $N_2O$ for the $N_2O$ decomposition reaction.

Figures 4a and 4b are Arrhenius-type plots for the NO + CO reaction on Rh and Pd catalysts, respectively. Apparent activation energies derived from these plots are presented in Table 2. Comparing the observed rates at 526 K gives relative turnover frequencies of 1, 3.2, 5.6, 7.5, 7.8, 34.8, and 235 for $Pd/Rh/Al_2O_3$, $Pd/Al_2O_3$, $Rh/Al_2O_3$, $Rh/CeO_x/Al_2O_3$, $Rh/La_2O_3/Al_2O_3$, $Pd/La_2O_3/Al_2O_3$, and $Pd/CeO_x/Al_2O_3$, respectively, for the NO + CO reaction. Clearly the ceria-promoted Pd catalyst is much more active than any of the other catalysts. Ceria also promoted the Rh catalyst while lanthana promoted only the Pd catalyst. For this reaction, the nitrogen-containing products are $N_2$ and $N_2O$. Figures 5a and 5b compare the dinitrogen selectivity for the Rh and Pd catalysts, respectively, as a function of temperature. Dinitrogen selectivity is defined as the rate of $N_2$ production divided by the rate of $N_2$ and $N_2O$ production. For both the Pd and Rh catalysts, the presence of ceria decreased the dinitrogen selectivity. In fact, the very active $Pd/CeO_x/Al_2O_3$ catalyst had the lowest $N_2$ selectivity (22%, independent of temperature). Lanthana had a minimal effect on the $N_2$ selectivity over Rh and a slightly deleterious effect over Pd.

The influence of reactant partial pressures on the rate of the NO + CO reaction at 483 K is summarized in Fig. 6 for $Rh/CeO_x/Al_2O_3$. The plot indicates a negative reaction order for CO partial pressure and a positive order for NO partial pressure. The lines represent a linear regression of the rate data which yield orders of $1.10 \pm 0.15$ for NO and $-0.29 \pm 0.15$ for CO (based on NO consumption). Results for the other catalysts are shown in Table 3. Reaction orders

**TABLE 2**

**Apparent Activation Energies for NO + CO, $N_2O$ + CO, and $N_2O$ Decomposition Reactions**

| | Apparent activation energy (kJ $mol^{-1}$) | | | | |
|---|---|---|---|---|---|
| | NO + CO | | $N_2O$ + CO | | $N_2O$ decomp, |
| Catalyst | This work | Literature value | This work | Literature value | This work |
| $Pd/Al_2O_3$ | 59.8 | 154 (15), 95.4 (31), 88.2 (32), 83.6 (33), 87.9 (16), 67.8 (18) | 104 | — | — |
| $Pd/CeO_x/Al_2O_3$ | 76.6 | — | 101 | — | — |
| $Pd/La_2O_3/Al_2O_3$ | 100 | — | 98.4 | — | — |
| $Rh/Al_2O_3$ | 86.6 | 117 (3), 101 (7) | 109 | 167 (5), 167 (34) | 139 |
| $Rh/CeO_x/Al_2O_3$ | 49.4 | 75.3 (3) | 139 | — | 157 |
| $Rh/La_2O_3/Al_2O_3$ | 150 | 126 (7) | 107 | — | 229 |
| $Pd/Rh/Al_2O_3$ | 100 | — | 129 | — | 118 |

*Note.* Numbers in parentheses refer to references.

**TABLE 3**

**Orders of Reaction for NO and CO**

| | | Reaction order | | | | | |
|---|---|---|---|---|---|---|---|
| | | NO consumption | | | | | |
| | | NO | | CO | | CO consumption | |
| Catalyst | $T$ (K) | This work | Literature value | This work | Literature value | NO | CO |
| $Pd/Al_2O_3$ | 553 | 1.02 | 0.50 (15) | −1.11 | −0.85 (15) | 0.86 | −0.88 |
| $Pd/CeO_x/Al_2O_3$ | 463 | * | — | −0.50 | — | 0.38 | −0.41 |
| $Pd/La_2O_3/Al_2O_3$ | 513 | * | — | * | — | — | — |
| $Rh/Al_2O_3$ | 533 | −0.03 | −0.37 (7), −0.14 (3) | 0.12 | 0.03 (7), 0.11 (3) | 0.02 | 0.04 |
| $Rh/CeO_x/Al_2O_3$ | 483 | 1.10 | 0.30 (3) | −0.29 | −0.19 (3) | 1.05 | −0.10 |
| $Rh/La_2O_3/Al_2O_3$ | 543 | −0.62 | −0.16 (7) | −0.01 | 0.04 (7) | — | — |
| $Pd/Rh/Al_2O_3$ | 573 | −0.02 | — | * | — | 0.10 | * |

*Note.* * indicates a maximum in the reaction order plot. Numbers in parentheses refer to references.

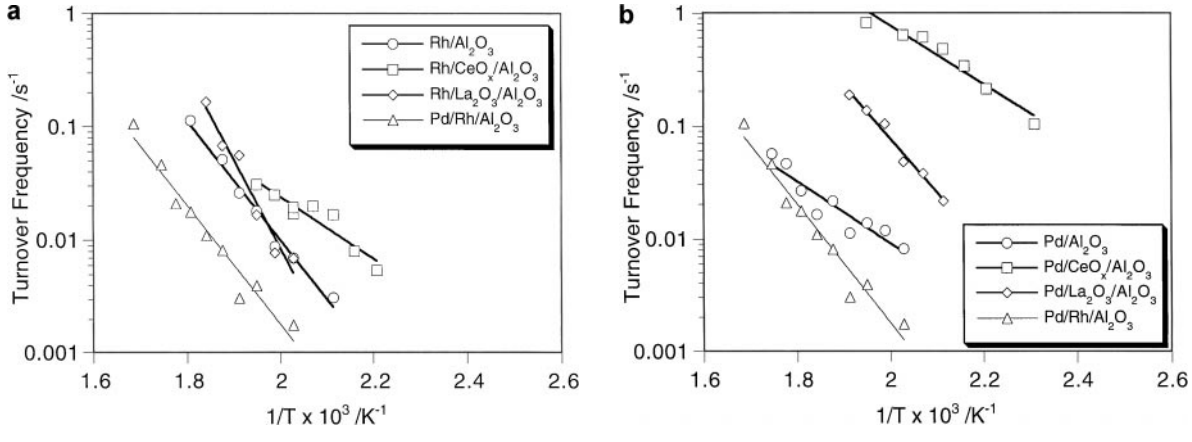


**FIG. 4.** Arrhenius-type plots for the NO + CO reaction over (a) $Rh/Al_2O_3$, $Rh/CeO_xAl_2O_3$, $Rh/La_2O_3/Al_2O_3$, and $Pd/Rh/Al_2O_3$ and (b) $Pd/Al_2O_3$, $Pd/CeO_x/Al_2O_3$, $Pd/La_2O_3/Al_2O_3$, and $Pd/Rh/Al_2O_3$ for reactant mixture of 5.07 kPa each of NO and CO.

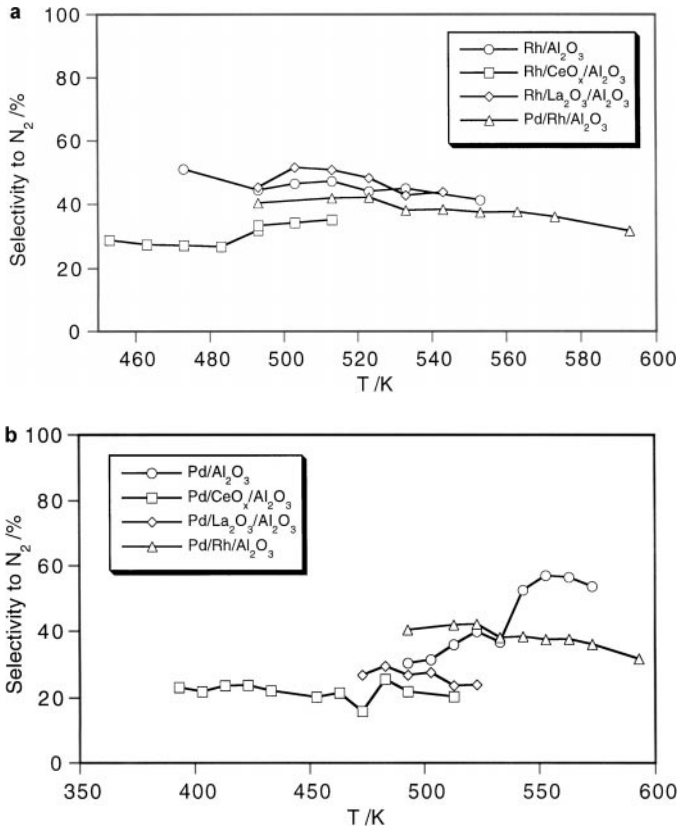


**FIG. 5.** $N_2$ selectivity vs temperature for the NO + CO reaction over (a) $Rh/Al_2O_3$, $Rh/CeO_xAl_2O_3$, $Rh/La_2O_3/Al_2O_3$, and $Pd/Rh/Al_2O_3$ and (b) $Pd/Al_2O_3$, $Pd/CeO_x/Al_2O_3$, $Pd/La_2O_3/Al_2O_3$, and $Pd/Rh/Al_2O_3$.

in Table 3 are shown for both NO and CO consumption. The reaction orders for the different reactants vary slightly due to different $N_2$ selectivities for the catalysts. Depending on the catalyst, the reaction order for NO varied from

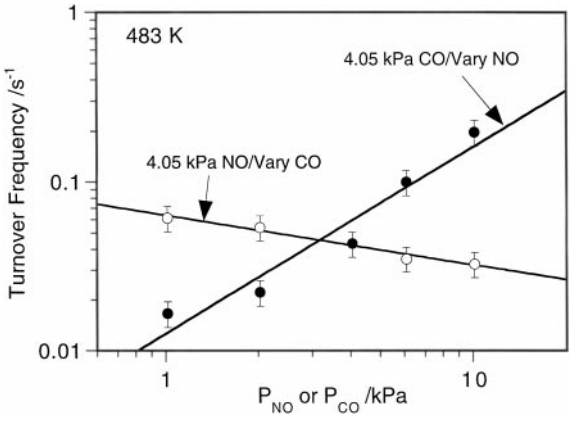


**FIG. 6.** Reaction order determination for the NO + CO reaction for $Rh/CeO_x/Al_2O_3$ at 483 K. The open circles are for a fixed $P_{NO} = 4.05$ kPa with a varying $P_{CO}$. The closed circles are for a fixed $P_{CO} = 4.05$ kPa with a varying $P_{NO}$.

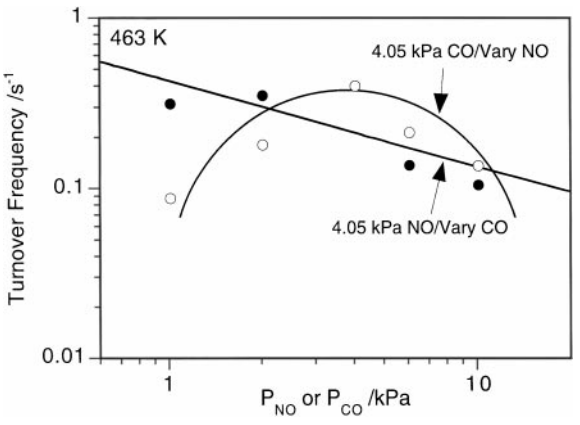


**FIG. 7.** Reaction order determination for the NO + CO reaction for $Pd/CeO_x/Al_2O_3$ at 463 K. The closed circles are for a fixed $P_{NO} = 4.05$ kPa with a varying $P_{CO}$. The open circles are for a fixed $P_{CO} = 4.05$ kPa with a varying $P_{NO}$.

about negative one-half to positive one. In addition, the reaction order for CO varied from about zero to negative one. Promotion of the metals by ceria dramatically altered the reaction orders. For instance, the presence of ceria on $Pd/Al_2O_3$ increased the CO reaction order from −1.11 to −0.50. However, for $Rh/Al_2O_3$, ceria increased the reaction order for NO from zero to 1.10 and decreased the CO reaction order from 0.12 to −0.29. For some catalysts, the reaction orders were positive at low partial pressures and negative at high partial pressures, over the range of conditions investigated. Figure 7 illustrates an example of this behavior for $Pd/CeO_x/Al_2O_3$. Interestingly, the maximum in rate occurred near equimolar concentrations of NO and CO for these samples.

Figures 8a and 8b are the Arrhenius-type plots for the $N_2O$ + CO reaction over the Rh and Pd catalysts, respectively. The ceria-promoted Pd catalyst again had the highest activity, but the promotional effect was not as dramatic as that seen for the NO + CO reaction. The relative turnover frequencies are 1, 1.3, 1.9, 7.8, 13.8, 14.2, and 42.2 for $Pd/Rh/Al_2O_3$, $Rh/La_2O_3/Al_2O_3$, $Rh/Al_2O_3$, $Pd/La_2O_3/Al_2O_3$, $Rh/CeO_x/Al_2O_3$, $Pd/Al_2O_3$, and $Pd/CeO_x/Al_2O_3$, respectively, at 555 K. The presence of lanthana slightly decreased the reaction rate on both Pd and Rh. The $N_2O$ molecule can also decompose in the absence of CO over Rh catalysts. The relative turnover frequencies for $N_2O$ decomposition without CO were 1, 2.6, 5.4, and 42.2 for $Pd/Rh/Al_2O_3$, $Rh/La_2O_3/Al_2O_3$, $Rh/Al_2O_3$, and $Rh/CeO_x/Al_2O_3$, respectively, at 573 K. Figure 9 shows the Arrhenius-type plots for this reaction. The decomposition of $N_2O$ under these reaction conditions in the absence of CO did not occur to any appreciable extent on $Pd/Al_2O_3$, $Pd/CeO_x/Al_2O_3$, and $Pd/La_2O_3/Al_2O_3$ over the 513–573 K temperature range. It was necessary to increase the temperature to about 673 K before $N_2O$ decomposed on those catalysts.

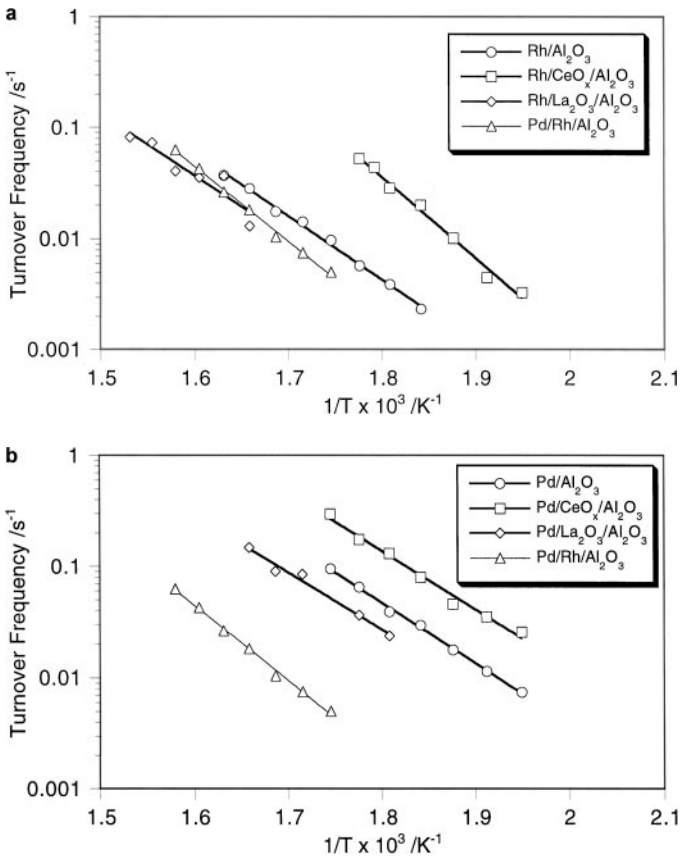


**FIG. 8.** Arrhenius-type plots for the $N_2O + CO$ reaction over (a) $Rh/Al_2O_3$, $Rh/CeO_xAl_2O_3$, $Rh/La_2O_3/Al_2O_3$, and $Pd/Rh/Al_2O_3$ and (b) $Pd/Al_2O_3$, $Pd/CeO_x/Al_2O_3$, $Pd/La_2O_3/Al_2O_3$, and $Pd/Rh/Al_2O_3$ for reactant mixture of 4.05 kPa each of $N_2O$ and CO.

Apparent activation energies for these two reactions ($N_2O + CO$, $N_2O$ decomposition) are presented in Table 2.

The influence of the reactant partial pressures on the rate of the $N_2O + CO$ reaction at 543 K is summarized

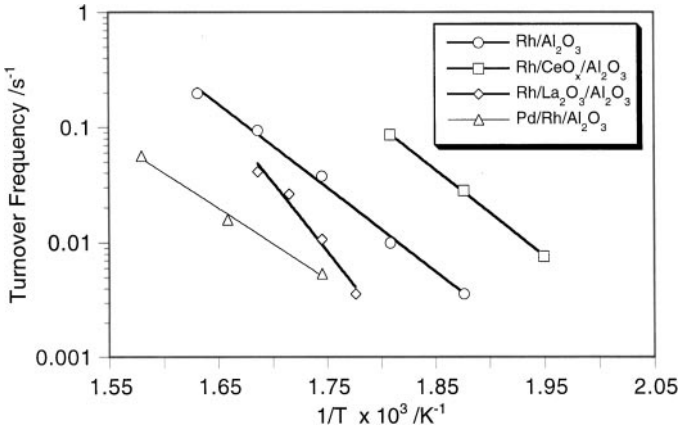


**FIG. 9.** Arrhenius-type plots for the $N_2O$ decomposition reaction over $Rh/Al_2O_3$, $Rh/CeO_x/Al_2O_3$, $Rh/La_2O_3/Al_2O_3$, and $Pd/Rh/Al_2O_3$ for 4.05 kPa $N_2O$.

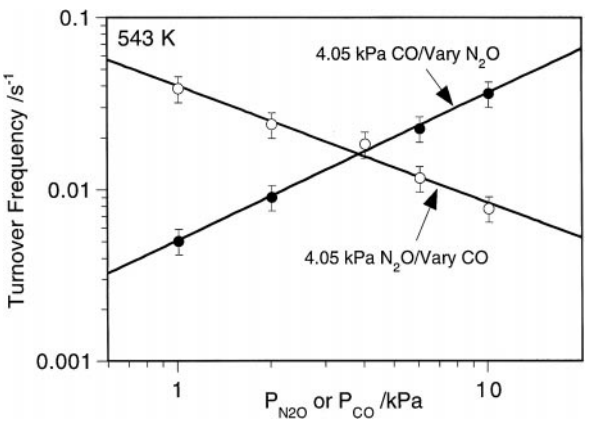


**FIG. 10.** Reaction order determination for the $N_2O + CO$ reaction for $Rh/CeO_x/Al_2O_3$ at 543 K. The open circles are for a fixed $P_{N_2O} = 4.05$ kPa with a varying $P_{CO}$. The closed circles are for a fixed $P_{CO} = 4.05$ kPa with a varying $P_{N_2O}$.

in Fig. 10 for $Rh/CeO_x/Al_2O_3$. The plot indicates a negative reaction order for CO partial pressure and a positive order for $N_2O$ partial pressure. The lines represent a linear regression of the rate data which yielded orders of $-0.68 \pm 0.15$ for CO and $0.86 \pm 0.15$ for $N_2O$. Results for the other catalysts are shown in Table 4. Reaction orders for $N_2O$ were positive and similar for all catalysts. Reaction orders for CO were negative for all catalysts, but the Pd catalysts were less inhibited by CO than the Rh catalysts. Ceria had little effect on the reaction order for either reactant whereas lanthana slightly decreased the $N_2O$ reaction order on Pd and slightly increased the CO reaction order on Rh.

Infrared spectroscopy was performed on catalysts to identify adsorbed species for the $N_2O + CO$ reaction. The Pd and Rh catalysts were exposed to $N_2O$, NO, and CO individually to determine the adsorption bands for each of these adsorbates. The reaction of $N_2O + CO$ was then performed on the catalysts at 573 K in the IR cell. Spectra for $Rh/Al_2O_3$, $Rh/CeO_x/Al_2O_3$, $Pd/Al_2O_3$, and $Pd/CeO_x/Al_2O_3$ in vacuum, after $N_2O + CO$ reaction, are shown in Fig. 11. For $Pd/Al_2O_3$, the major absorption band in the 1700–2500-$cm^{-1}$ range is a small band at 1907 $cm^{-1}$ and is attributed to bridged carbonyl (24). A similar bridged carbonyl species at 1887 $cm^{-1}$ was observed for $Pd/CeO_x/Al_2O_3$ (24). For $Rh/Al_2O_3$, a strong band at 2024 $cm^{-1}$ indicates either a dicarbonyl or a triply bonded carbonyl (25). In contrast to the species observed on the Pd catalysts, there were also bands at 1895 $cm^{-1}$ for either a cationic NO or bridged carbonyl species (25), and a strong band at 2251 $cm^{-1}$ attributed to isocyanate (–NCO) on the alumina support (26–28). Finally, for $Rh/CeO_x/Al_2O_3$, the spectrum is simpler with a bridged carbonyl at 1855 $cm^{-1}$, and a dicarbonyl or tricarbonyl species at 2005 $cm^{-1}$ (exact assignment of this peak is unclear; however, it is clearly a CO peak based on reference spectra).

**TABLE 4**

**Orders of Reaction for $N_2O$ and CO**

| Catalyst | $T$ (K) | Reaction order | | | |
|---|---|---|---|---|---|
| | | $N_2O$ | | CO | |
| | | This work | Literature value | This work | Literature value |
| $Pd/Al_2O_3$ | 543 | 0.69 | — | −0.32 | — |
| $Pd/CeO_x/Al_2O_3$ | 553 | 0.62 | — | −0.31 | — |
| $Pd/La_2O_3/Al_2O_3$ | 583 | 0.46 | — | −0.35 | — |
| $Rh/Al_2O_3$ | 593 | 0.72 | 0.65 (5), 1.14 (34) | −0.86 | −1.0 (5), −1.18 (34) |
| $Rh/CeO_x/Al_2O_3$ | 543 | 0.86 | — | −0.68 | — |
| $Rh/La_2O_3/Al_2O_3$ | 643 | 0.76 | — | −0.48 | — |
| $Pd/Rh/Al_2O_3$ | 613 | 0.80 | — | −0.37 | — |

*Note.* Numbers in parentheses refer to references.

## DISCUSSION

### *NO + CO Reaction*

The kinetic results clearly showed that the presence of ceria increases the reaction rate, decreases the dinitrogen selectivity, and alters the NO + CO reaction orders over both Pd and Rh. Even though the reaction orders over Pd and Rh were affected by the presence of lanthana, the specific activity was promoted only in the case of Pd. The implications of these results are discussed below and a kinetic model for the reaction is developed.

The turnover frequency for the ceria-promoted Pd was approximately 2 orders of magnitude greater than that for the unpromoted Pd. Promotion of Rh with ceria produced a much smaller increase in the turnover frequency, about 50%. For lanthana, the specific reaction rate increased by 1 order of magnitude on supported Pd, yet the rate on supported Rh was barely affected at our reaction conditions. The promotional effect of the ceria (and lanthana) cannot be attributed to the increased metal dispersion since activity for both Rh and Pd has been shown previously to decrease with increasing dispersion (8, 15). Although alumina-supported ceria catalyzed the NO + CO reaction with no metal present, the reaction rate, on a per gram basis, was a factor of 4 lower than that with any other catalyst studied in this work. In addition, reaction rates on pure lanthana/alumina were an order of magnitude below those on ceria/alumina. Therefore, the enhancement in observed rates is due to either a modification of the metal particles or creation of new sites at the metal/promoter interface. The promotional effect of ceria (and lanthana) cannot be explained simply by the additional promoter surface area.

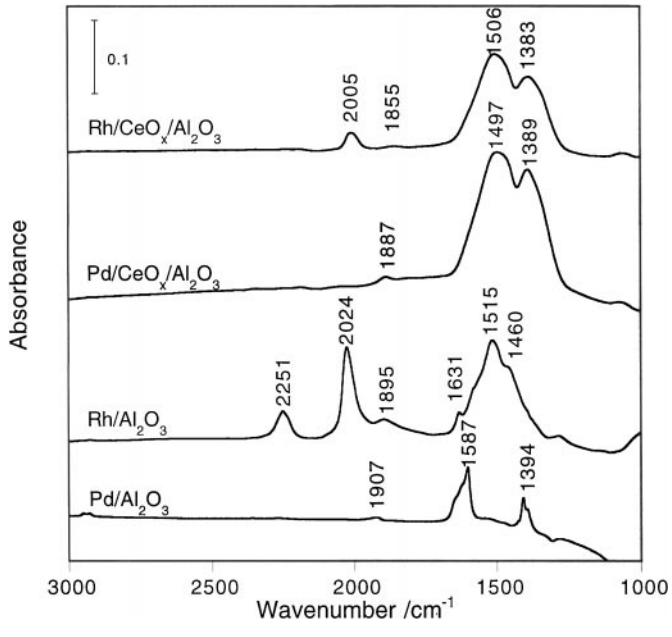


**FIG. 11.** Infrared spectra of $Pd/Al_2O_3$, $Rh/Al_2O_3$, $Pd/CeO_x/Al_2O_3$, and $Rh/CeO_x/Al_2O_3$ under vacuum at 573 K after the $N_2O$ + CO reaction.

The effects of ceria and lanthana on apparent activation energy, $N_2$ selectivity, and reaction order for Rh were similar to those previously reported in the literature (3, 7, 29, 30). Literature values for apparent activation energy and reaction order are shown in Tables 2 and 3, respectively (16, 31–33). The only difference is that Oh found similar $N_2$ selectivity over both $Rh/Al_2O_3$ and $Rh/CeO_x/Al_2O_3$ whereas we observed a decrease in selectivity with addition of ceria. For unpromoted Pd, apparent activation energy, $N_2$ selectivity, and reaction order were similar to those reported by Rainer *et al.* (15, 18). The effects of ceria and lanthana promoters on $N_2$ selectivity and reaction order for Pd were similar; in contrast, the apparent activation energy on Pd decreased with ceria promotion and increased with lanthana promotion.

*Proposed reaction sequence.* For the reaction of NO + CO, our experimental results and previous works (3, 4, 6, 18, 20, 29, 30, 34) suggest the reaction can be represented

by the following set of elementary steps:

$$CO + S \Leftrightarrow CO_a \quad [4]$$

$$NO + S \Leftrightarrow NO_a \quad [5]$$

$$NO_a + S \rightarrow N_a + O_a \quad [6]$$

$$NO_a + N_a \rightarrow N_2O + 2S \quad [7]$$

$$N_a + N_a \rightarrow N_2 + 2S \quad [8]$$

$$CO_a + O_a \rightarrow CO_2 + 2S, \quad [9]$$

where "S" denotes a surface site and the subscript "a" denotes an adsorbed species.

An additional elementary reaction step,

$$NO_a + N_a \rightarrow N_2 + O_a + S, \quad [10]$$

has been proposed previously to provide an alternative path for $N_2$ formation at low temperatures (6). However, Belton *et al.* have shown that $NO_a$ and $N_a$ react on Rh to form only $N_2O$ and that $N_2$ formation at low temperature occurs only by N atom recombination (34). For Pd, Rainer *et al.* (18) and Almusaiteer and Chuang (20) have also proposed mechanisms without this alternative $N_2$ formation pathway. Therefore, we have not included this step in our mechanism.

The development of a kinetic model assumes that the presence of ceria or lanthana did not change the basic reaction mechanism, but instead altered the rates of the individual elementary steps. We have shown that both alumina- and ceria/alumina-supported Pd and Rh are also capable of further reducing $N_2O$ with CO to $N_2$ and $CO_2$. However, under our conditions, the rate of the $N_2O + CO$ reaction was at least 1 order of magnitude lower than the rate of the $NO + CO$ reaction, and the actual amount of $N_2O$ produced was small due to the low levels of conversion. Additionally, experiments with isotopically labeled $N_2O$ over Rh(111) (35) and varying concentrations of $N_2O$ in the feed over $Pt_{10}Rh_{90}$(111) (36) have not provided any evidence of $N_2O$ readsorption and reaction to form $N_2$. Consequently, steps involving readsorption and surface reaction of $N_2O$ have not been incorporated into the proposed mechanism.

A kinetic analysis of the $NO + CO$ reaction over silica-supported Rh by Hecker and Bell (4) indicates that when the dissociation of NO (reaction [6]) is the rate-determining step, the catalyst is predominately covered with molecularly adsorbed NO. Thus, a negative first-order dependence on NO partial pressure is anticipated. After studying Rh supported on alumina and ceria/alumina, Oh (3) concluded that weakly negative or moderately positive reaction orders in NO suggest that the NO dissociation reaction is not rate determining. Additional work by Oh *et al.* (6) demonstrated that when the NO dissociation rate is reasonably rapid, the catalyst surface is largely covered with both adsorbed nitrogen atoms and molecularly adsorbed NO. Finally, for a positive one-half reaction order in NO, Rainer *et al.* have concluded that the dissociation of NO is not the rate-determining step on Pd but instead the removal of thermally stable atomic nitrogen species is more important (15). The results in Table 3 indicate all of the above cases. This variety of reaction orders indicates that different elementary reactions may be rate determining under different conditions. Thus, we develop a rate expression without assuming a single rate-determining step. The overall rate of NO consumption is given by

$$r_{NO} = 2r_{N_2O} + 2r_{N_2}, \quad [11]$$

where $r_{N_2}$ and $r_{N_2O}$ denote the rates of $N_2$ and $N_2O$ formation depicted in reactions [7] and [8]. The rates $r_{N_2}$ and $r_{N_2O}$ can be expressed in terms of the fractional surface coverages ($\theta$) of the adsorbed species as

$$r_{N_2} = k_8\theta_N^2 \quad [12]$$

$$r_{N_2O} = k_7\theta_{NO}\theta_N, \quad [13]$$

where $k_7$ and $k_8$ are the rate constants for reactions [7] and [8], respectively. Substitution of Eqs. [12] and [13] into Eq. [11] yields

$$r_{NO} = 2\left[k_7\theta_{NO}\theta_N + k_8\theta_N^2\right]. \quad [14]$$

Equilibrium adsorption relationships are used to determine $\theta_{NO}$ and $\theta_{CO}$:

$$\theta_{NO} = K_5P_{NO}\theta_V \quad [15]$$

$$\theta_{CO} = K_4P_{CO}\theta_V. \quad [16]$$

The overall site balance is given by

$$1 = \theta_{NO} + \theta_N + \theta_{CO} + \theta_V, \quad [17]$$

where $\theta_V$ is the fraction of vacant sites. Determination of $\theta_N$ requires a nitrogen surface balance and the pseudo-steady state hypothesis:

$$r_N = k_6\theta_{NO}\theta_V - k_7\theta_{NO}\theta_N - k_8\theta_N^2 = 0 \quad [18]$$

Equation [18] can then be solved for $\theta_N$:

$$\theta_N = N\theta_V \quad [19]$$

with

$$N = \left(\frac{-k_7K_5P_{NO} + [(k_7K_5P_{NO})^2 + 4k_8k_6K_5P_{NO}]^{1/2}}{2k_8}\right). \quad [20]$$

Substitution of [15] through [20] into [14] yields the rate expression for NO consumption:

$$r_{NO} = 2\left[\frac{k_7K_5P_{NO}N + k_8N^2}{(1 + K_5P_{NO} + K_4P_{CO} + N)^2}\right]. \quad [21]$$

Even though the resulting expression is complex, the important consequence is that the observed NO reaction order

can be either positive, negative, or zero depending on the relative surface coverages of intermediates.

For high surface coverage of NO, the rate will exhibit a negative NO reaction order. However, if the surface coverage of adsorbed N atoms is high, the rate will exhibit a NO reaction order of about zero. Intermediate surface coverages of NO and $N_a$ or high CO coverage results in a positive NO reaction order. This model can also easily explain the results on $Pd/CeO_x/Al_2O_3$, which indicate a maximum in the reaction order plot, by noting that high CO coverage at low NO partial pressure results in a positive NO reaction order. Increasing NO surface coverage as the NO partial pressure increases causes the reaction order to become negative.

We found that the selectivity to $N_2$ generally decreased as NO partial pressure (and thus NO surface coverage) increased. Clearly, the relative surface coverage of NO and N depends on the ability of the catalyst to dissociate NO. The affinity of Pd and Rh to dissociate NO can be contrasted by comparing reaction energetics obtained on single crystals at low coverages. For Rh, $E_{dis} = 73.2$ kJ mol$^{-1}$ with $A = 2.1 \times 10^{10}$ s$^{-1}$ and, for Pd, $E_{dis} = 115.7$ kJ mol$^{-1}$ with $A = 4 \times 10^{11}$ s$^{-1}$ (34, 37). Although $E_{dis}$ depends on NO surface coverage, in both cases NO dissociation rates decrease similarly as NO coverage increases. Therefore, at 500 K, NO dissociates approximately $10^3$ times faster on Rh than Pd. This high NO dissociation rate should correspond to higher relative surface coverages of adsorbed N atoms on Rh. Examination of our experimental results on $Rh/Al_2O_3$ shows that the NO + CO reaction is essentially zero order in both NO and CO, indicating that there are moderate to high coverages of both NO and $N_a$. For Pd, where dissociation is less energetically favored, reaction orders are +1.02 in NO and −1.11 in CO. The negative CO reaction order indicates that the surface coverage is dominated by adsorbed CO, which leads to a low activity for NO reactions on Pd. Again, the similar low surface coverages of both NO and $N_a$ lead to similar amounts of $N_2$ and $N_2O$ formed, which agrees with the results of 50% $N_2$ selectivity at 550 K.

When ceria is added to the support, the turnover frequency is increased for both Rh and Pd catalysts. An understanding of the interaction among ceria, transition metal, and adsorbed species is required to explain this increased activity. One possible explanation of the promotional effect has been proposed by Oh (3). In his mechanism, NO adsorbs near the metal/ceria interface with the nitrogen end of the molecule attached to the metal and the oxygen end attached to an oxygen-deficient cerium species. The concurrent interaction of both ends of the NO molecule with the catalyst surface should weaken the N–O bond and facilitate dissociation. The increased activity of the ceria-promoted catalysts may also be partially due to the ability of ceria to store this removed oxygen in the lattice. This explanation of enhanced NO dissociation in the presence of ceria is consistent with the measured reaction orders in this work. Enhanced NO dissociation should decrease the steady-state $NO_a$ surface coverage and increase the NO reaction order, which is observed for $Rh/CeO_x/Al_2O_3$.

For $Pd/CeO_x/Al_2O_3$ under stoichiometric conditions, enhanced NO dissociation increases the coverage of N atoms. Moreover, additional oxygen atoms from dissociated NO contribute to higher CO oxidation rates and lower surface coverages of CO, thus increasing the CO reaction order. With fewer adsorbed CO molecules present, the coverage of adsorbed NO increases, which results in higher $N_a$ coverage due to enhanced dissociation and a decreased reaction order. The result that $N_2$ and $N_2O$ production rates are both enhanced by the presence of the promoter is consistent with the postulate that the interface produces more N atoms.

The presence of ceria did not lead to a dramatic increase in activity of Rh since NO dissociation is readily accomplished by the Rh metal itself. Even though ceria did indeed promote the reaction over Rh, the combination of metal and promoter may dissociate NO too well, thus decreasing the coverage of adsorbed NO to the point where there is not enough adsorbed NO to react with the $N_a$. The surface is effectively blocked by adsorbed N atoms. This situation is consistent with our results on $Rh/CeO_x/Al_2O_3$ since the NO reaction order was 1.10 and the CO reaction order was slightly negative.

For the lanthana-promoted catalysts, the reaction was enhanced on Pd and was essentially unchanged on Rh. Thus, an important interaction between the Pd and lanthana is indicated. We propose a mechanism similar to that described above. First, NO adsorbs at the metal/oxide interface. In this case, an interaction between the oxygen of NO with oxophilic Lewis acid sites on the surface such as the $La^{3+}$ cation may be responsible for weakening the N–O bond. This explanation is qualitatively the same as that proposed by Alvero *et al.* for enhanced CO dissociation over a lanthana-promoted rhodium/alumina catalyst (38). Any improvement in N–O bond dissociation provided by the support would quickly result in rapid product formation as discussed earlier.

### *$N_2O$ + CO Reaction*

For both Pd and Rh, the presence of ceria increased the reaction rates by about 0.5 order of magnitude when compared to the unpromoted catalysts. Similar to the NO + CO reaction, ceria-promoted Pd exhibited the highest activity. When compared to the NO + CO reaction under similar conditions, rates for the $N_2O$ + CO reaction on the same catalyst (Pd or Rh) were lower by 0.5 to 2 orders of magnitude. Additionally, for the Rh catalysts, inhibition of the rate of $N_2O$ reaction by CO clearly demonstrates that CO occupied a large fraction of the available surface sites and suppressed $N_2O$ adsorption and decomposition. In contrast to

results with ceria, no promotional effect was observed with lanthana; in fact, reaction rates on lanthana-promoted Pd and Rh were lower by a factor of 2. This may be attributed to the lower metal dispersion of the lanthana-promoted catalysts. Alumina-supported ceria (without any transition metal) also catalyzed the $N_2O + CO$ reaction, but the reaction rate on a per gram basis was lower by a factor of 2 than that for any other catalyst. Therefore, similar to the $NO + CO$ reaction, the observed rates are due to either the metal or ceria in contact with the metal.

The presence of ceria and lanthana did not have as dramatic an effect on the kinetic parameters for the $N_2O + CO$ reaction as for the $NO + CO$ reaction. With the exception of ceria-promoted Rh, the promoter had very little effect on apparent activation energy. Literature values for unpromoted Rh are given in Table 2 (5, 9). Likewise, the $N_2O$ and CO reaction orders are in general agreement with the literature values in Table 4. We have not been able to find analogous studies on Pd catalysts and promoted Rh catalysts. It is interesting to note that ceria had little effect on reaction orders but the CO reaction order was significantly different on the two metals.

In an attempt to gain insight into the elementary steps involved in the $N_2O + CO$ reaction, we performed *in situ* IR spectroscopy on samples previously exposed to the reactant gases. As expected for weakly adsorbing $N_2O$ and strongly adsorbing CO, the majority of the observed absorption bands were attributed to carbonate on the support and carbonyls on the metal. No $N_2O$ absorption bands were observed. For the $Rh/Al_2O_3$ catalyst, the isocyanate band at 2251 $cm^{-1}$ indicates the presence of adsorbed nitrogen atoms on the surface. Interestingly, adsorption and decomposition of $N_2O$ without CO on this catalyst did not reveal the presence of NO on the surface. Isocyanate (–NCO) is formed by the reaction between an adsorbed nitrogen atom and CO (39, 40). The presence of isocyanate on $Rh/Al_2O_3$ indicates that $N_2O$ decomposes in the presence of CO to form adsorbed NO and N atoms. This mechanism has recently been proposed by Uner to describe the kinetics of the $N_2O + CO$ reaction over Rh surfaces (41). Previous studies have shown that for alumina-supported noble metals (including Pd and Rh), the isocyanate species forms from NO and CO on the metal and subsequently migrates to the support (28, 40). Once on the support, the isocyanate is quite stable and is not readily decomposed. These studies have also indicated that the surface coverage of isocyanate is greatest under conditions of high CO and low NO surface coverages as would be the case during the $N_2O + CO$ reaction. Additionally, isocyanate forms at similar rates under similar conditions from NO and CO on both Pd and Rh (28). For ceria-supported catalysts, formation of isocyanate requires different surface conditions. In that case, isocyanate formation occurs when the surface is first covered by NO and then exposed to CO (25).

Since the evidence in this work indicates that both adsorbed nitrogen atoms and NO are present on the surface for $Rh/Al_2O_3$ and not on the $Pd/Al_2O_3$ surface, the potential exists for the reaction to occur by two separate mechanisms over the two different metals. If adsorbed $N_2O$ were to dissociate into $NO_a$ and $N_a$, the high CO surface coverage would allow for ready formation of isocyanate, which would then migrate to the alumina support. The high surface area alumina support acts as an isocyanate trap, which allows for easy interrogation by IR spectroscopy. The presence of isocyanate therefore serves as a marker for the $N_2O$ reaction into $NO_a$ and $N_a$. The lack of a similar isocyanate marker on the $Pd/Al_2O_3$ catalyst indicates that this $N_2O$ decomposition path is not occurring to any significant extent. For the ceria-supported catalysts, the lack of the isocyanate marker for both metals is expected since high NO coverage is required for isocyanate formation (25). The high NO coverage required for isocyanate formation is not achieved due to the presence of CO. Therefore, for the ceria-promoted catalysts, infrared spectroscopy does not provide conclusive evidence for either $N_2O$ decomposition mechanism. However, when the IR spectroscopy results are combined with reaction kinetics, we conclude that, although the two unpromoted metals may have different reaction mechanisms for $N_2O$ decomposition, the presence of ceria did not appreciably change the observed reaction orders and likely did not change the mechanism.

*Proposed reaction sequence.* Based on our experimental results and those in the literature (5, 9, 41), models for $N_2O + CO$ reaction are developed below. In the mechanism given below, $N_2O$ dissociates in two successive steps to give adsorbed N atoms, which recombine to $N_2$:

$$N_2O_{(g)} + S \Leftrightarrow N_2O_a \quad [22]$$

$$N_2O_a + S \Leftrightarrow N_a + NO_a \quad [23]$$

$$NO_a + S \rightarrow N_a + O_a \quad [24]$$

$$2N_a \rightarrow N_{2(g)} + 2S. \quad [25]$$

Using the above set of elementary reactions, the overall rate expression is (see Ref. (41), for a complete development of the expression):

$$r_{N_2O+CO} = \left(k_{NO}^{diss} k_{N_2}^{1/2} K_{N_2O} K_{N_2O}^{diss}\right)^{2/3} K_{CO}^{-1} \left(P_{N_2O}^{2/3} / P_{CO}\right), \quad [26]$$

where $k_{NO}^{diss}$ and $k_{N_2}$ are the rate constants for Eqs. [24] and [25], respectively, and $K_{N_2O}^{diss}$ is the equilibrium constant for Eq. [23].

Similar to the $NO + CO$ reaction, the promotional effects of the supports can be understood by contrasting the experimental results for the different catalysts and comparing results from the $NO + CO$ reactions. For the two-step mechanism, the rate-determining step is assumed to be the dissociation of adsorbed NO. Comparing the two promoters for this reaction, ceria increased activity while lanthana

did not. Since ceria produced a similar promotional effect for the NO + CO reaction where NO dissociation was the important step, a parallel explanation for the $N_2O$ + CO reaction can be provided. As discussed above, ceria provides metal/interface sites for NO adsorption and dissociation. Results from IR spectroscopy indicate that this mechanism may occur on Rh catalysts. Consistent with the NO + CO results, lanthana demonstrated no promotional effect for the $N_2O$ + CO reaction, again indicating no ability to enhance NO dissociation on Rh.

An alternative sequence to form $N_2$ by $N_2O$ dissociation in one step is represented by the following set of reactions:

$$N_2O_{(g)} + S \Leftrightarrow N_2O_a \quad [27]$$

$$N_2O_a \rightarrow N_{2(g)} + O_a \quad [28]$$

$$CO + S \Leftrightarrow CO_a \quad [29]$$

$$CO_a + O_a \rightarrow CO_{2(g)} + 2S. \quad [30]$$

From these reactions we can see that the rate of the $N_2O$ + CO reaction is given by

$$r_{N_2O+CO} = k_{diss}\theta_{N_2O} = k_r\theta_{CO}\theta_O, \quad [31]$$

where $k_{diss}$ and $k_r$ are the rate constants for Eqs. [28] and [30], respectively. The appropriate terms for the fractional surface coverage of $N_2O$ are developed using the equilibrium relationships for the adsorption of $N_2O$ and CO, an overall site balance, and the pseudo-steady-state hypothesis. Assuming that surface coverage of atomic oxygen is small, the fractional surface coverage of $N_2O$ is

$$\theta_{N_2O} = \frac{K_{N_2O}P_{N_2O}}{1 + K_{N_2O}P_{N_2O} + K_{CO}P_{CO}}. \quad [32]$$

This is substituted into Eq. [31] to yield the overall reaction rate expression

$$r_{N_2O+CO} = \frac{k_{diss}K_{N_2O}P_{N_2O}}{1 + K_{N_2O}P_{N_2O} + K_{CO}P_{CO}}. \quad [33]$$

If the decomposition step described by [28] requires an adjacent vacant site, the form of the rate expression is similar to [33] except the denominator is squared.

The proposed $N_2O$ + CO one-step reaction mechanism does not contain the same NO dissociation reaction as the two-step mechansim. Therefore, a different explanation of the ceria promotional effect is required. The proposed mechanism requires simple $N_2O$ adsorption with subsequent dissociation to leave behind an adsorbed O for CO oxidation. This is similar to the $N_2O$ decomposition reaction observed on Rh(111) in the absence of CO (42), Cu(111) (43), Ni(110) (44) and is consistent with our IR spectroscopy results. The important step in this mechanism is the $N_2O$ decomposition reaction (Eq. [28]) and it likely involves the ceria promoter. For $N_2O$ decomposition without CO, Cunningham *et al.* have attributed the increased activity with ceria to sites with excess electrons at the metal/ceria interface. This provides storage sites for the dissociated O atoms until another O atom is available to scavenge the oxygen and complete the redox cycle (45). Again, the ceria may also store this oxygen internally. For the $N_2O$ + CO reaction, the CO scavenges the stored oxygen. Based on the lack of an isocyanate marker in the IR spectroscopy, we conclude that the one-step mechanism is occurring on the Pd catalysts. It should also be noted that the one-step mechanism may also contribute to some activity on the Rh catalysts. Similar to Rh, lanthana did not promote the $N_2O$ + CO reaction over Pd. This is a clear example of the ability of ceria to promote a reaction by virtue of its ability to easily cycle between oxidation states. Lanthana is not capable of easily changing oxidation states under these conditions.

We also studied the $N_2O$ decomposition reaction in the absence of CO and found that (1) $N_2O$ will not decompose over the $Pd/Al_2O_3$, $Pd/CeO_x/Al_2O_3$, and $Pd/La_2O_3/Al_2O_3$ catalysts at the reaction temperatures used here (513–573 K) and (2) the presence of ceria increased the rate of $N_2O$ decomposition while lanthana slightly decreased the rate of $N_2O$ decomposition on Rh containing catalysts.

Consistent with our results on the inability of Pd to catalyze the $N_2O$ decomposition, Isa and Saleh reported that, after initial oxidation, Pd did not tend to adsorb further $N_2O$ between 303 and 523 K (46). Li and Armor have also shown that for similar conversion, $N_2O$ decomposition on $Pd/Al_2O_3$ requires a temperature approximately 150 K higher than that of $Rh/Al_2O_3$ (47). Our results show that a temperature of greater than 663 K was required for a 3% conversion of $N_2O$. This observation agrees with that of Redmond, who determined a rate expression for $N_2O$ decomposition at elevated temperatures (1013–1217 K) and demonstrated that the reaction is poisoned by adsorbed oxygen (48). For our Pd catalysts, the fresh sample appears to decompose enough $N_2O$ to oxidize the surface and then no further reaction of $N_2O$ occurs.

For the Rh catalysts, the rate of consumption of $N_2O$ was faster in the absence of CO. The $N_2O$ decomposition reaction, in the absence of CO, cannot simply be ascribed to the presence of alumina or ceria/alumina support since temperatures of 753 and 713 K, respectively, were necessary to begin $N_2O$ decomposition on these supports without transition metals. Similar to both the NO + CO and $N_2O$ + CO reactions, the presence of ceria served to increase the rate of $N_2O$ decomposition over Rh by approximately 1 order of magnitude.

*$NO_x$ reactions on the bimetallic catalyst.* For the NO + CO reaction, the turnover frequency on $Pd/Rh/Al_2O_3$ was lower than that on either $Pd/Al_2O_3$ or $Rh/Al_2O_3$, which demonstrates that there is no synergistic effect when two metals are combined. Interestingly, the apparent activation energy and reaction orders on $Pd/Rh/Al_2O_3$ were similar

to those on $Rh/Al_2O_3$. For the $N_2O + CO$ reaction, the turnover frequency on $Pd/Rh/Al_2O_3$ was an order of magnitude lower than that on $Pd/Al_2O_3$, but within a factor of 2 of that on $Rh/Al_2O_3$. The combined kinetic results of $NO_x$ reactions suggest that the surface properties of the bimetallic sample are dominated by Rh. The lack of formation of a Pd $\beta$-hydride phase during dihydrogen chemisorption on $Pd/Rh/Al_2O_3$ is consistent with this hypothesis.

## CONCLUSIONS

This paper describes the results of a comparative kinetic study of the $NO + CO$, $N_2O + CO$, and $N_2O$ decomposition reactions over alumina-, ceria/alumina-, and lanthana/alumina-supported Pd and Rh catalysts. Since no synergistic effect was found for $NO_x$ reduction on a Pd/Rh bimetallic sample, monometallic catalysts were the focus of this study. For the $NO + CO$ reaction, the changes in kinetic parameters between alumina-, ceria/alumina-, and lanthana/alumina-supported Rh agree qualitatively with those previously reported in the literature for apparent activation energies and reaction orders. Comparable studies on promoted Pd catalysts are unavailable. In the current work, the ceria/alumina-supported Pd catalyst exhibited activity for the $NO + CO$ reaction an order of magnitude greater than that of ceria/alumina-supported Rh. The lanthana/alumina-supported Pd catalyst was the second most active. Additionally, the presence of ceria and lanthana had a large effect on the kinetic parameters over both Rh and Pd. However, these effects were not consistent on both catalysts. The ceria and lanthana promoters appear to affect the $NO + CO$ reaction by facilitating the dissociation of NO at the metal/promoter interface. This explanation can account for the altered activities, reaction orders, and dinitrogen selectivities of the promoted catalysts. In addition, the ceria/metal interface appeared to dissociate NO more effectively than the lanthana/metal interface.

Although the presence of ceria increased the rate of the $N_2O + CO$ reaction on both Pd and Rh, it had very little effect on apparent activation energies and reaction orders. Lanthana had no effect on activities or activation energies. Based on infrared spectroscopy and reaction order data, the $N_2O + CO$ reaction occurred via different mechanisms on Rh and Pd. The reaction on Rh appeared to involve $N_2O$ dissociating into N and NO with subsequent dissociation of NO. For Pd, $N_2O$ appeared to react directly to $N_2$ and adsorbed oxygen.

## ACKNOWLEDGMENTS

This work was supported by the Division of Chemical Sciences, Office of Basic Energy Sciences, Office of Energy Research, U.S. Department of Energy. Additional support was provided by the Virginia Academic Enhancement Program.

## REFERENCES

1. Taylor, K. C., *Catal. Rev.-Sci. Eng.* **35**, 457 (1993).
2. Cho, B. K., Shanks, B. H., and Bailey, J. E., *J. Catal.* **115**, 486 (1989).
3. Oh, S. H., *J. Catal.* **124**, 477 (1990).
4. Hecker, W. C., and Bell, A. T., *J. Catal.* **84**, 200 (1983).
5. McCabe, R. W., and Wong, C., *J. Catal.* **121**, 422 (1990).
6. Oh, S. H., Fisher, G. B., Carpenter, J. E., and Goodman, D. W., *J. Catal.* **100**, 360 (1986).
7. Pande, N. T., and Bell, A. T., *J. Catal.* **98**, 7 (1986).
8. Oh, S. E., and Eickel, C. C., *J. Catal.* **128**, 526 (1991).
9. Belton, D. N., and Schmeig, S. J., *J. Catal.* **138**, 70 (1992).
10. Trovarelli, A., de Leitenburg, C., and Dolcettis, G., *Chemtech* 32 (1997).
11. Huang, S.-J., Walters, A. B., and Vannice, M. A., *J. Catal.* **173**, 229 (1998).
12. Muraki, H., Shinjoh, H., Sobukawa, H., Yokata, K., and Fujitani, Y., *Ind. Eng. Chem., Prod. Res. Dev.* **25**, 202 (1986).
13. Muraki, H., Shinjoh, H., and Fujitani, Y., *Appl. Catal.* **22**, 325 (1986).
14. Steel, M. C. F., *in* "Catalysis and Automotive Pollution Control II" (A. Crucq, Ed.), Vol. 71, p. 105. Elsevier, Brussels, Belgium, 1991.
15. Rainer, D. R., Vesecky, S. M., Oh, W. S., and Goodman, D. W., *J. Catal.* **167**, 234 (1997).
16. Vesecky, S. M., Chen, P., Xu, X., and Goodman, D. W., *J. Vac. Sci. Technol. A* **13**, 1539 (1995).
17. Vesecky, S. M., Rainer, D. R., and Goodman, D. W., *J. Vac. Sci. Technol. A* **14**, 1457 (1996).
18. Rainer, D. R., Koranne, M., Vesecky, S. M., and Goodman, D. W., *J. Phys. Chem. B* **101**, 10769 (1997).
19. Almusaiteer, K., and Chuang, S. S. C., *J. Catal.* **180**, 161 (1998).
20. Almusaiteer, K., and Chuang, S. S. C., *J. Catal.* **184**, 189 (1999).
21. Kenvin, J. C., White, M. G., and Mitchell, M. B., *Langmuir* **7**, 1198 (1991).
22. Shi, C., Walters, A. B., and Vannice, M. A., *Appl. Catal. B* **14**, 175 (1997).
23. Benson, J. E., Hwang, H. S., and Boudart, M., *J. Catal.* **30**, 146 (1973).
24. Vannice, M. A., *in* "Catalysis Science and Technology" (J. R. Anderson and M. Boudart, Eds.), Vol. 3, p. 139. Springer-Verlag, Berlin, 1982.
25. Keiski, R. L., Harkonen, M., Lahti, A., Maunula, T., Savimaki, A., and Slotte, T., *in* "Catalysis and Automotive Pollution Control III" (A. Frennet and J.-M. Bastin, Eds.), Vol. 96, p. 85. Elsevier, Amsterdam, 1995.
26. Unland, M., *J. Catal.* **31**, 459 (1973).
27. Solymosi, F., and Bansagi, T., *J. Phys. Chem.* **83**, 552 (1979).
28. Solymosi, F., Volgyesi, L., and Rasko, J., *Z. Phys. Chem.* **79**, 79 (1980).
29. Cho, B. K., *J. Catal.* **148**, 697 (1994).
30. Peden, C. H. F., Belton, D. N., and Schmeig, S. J., *J. Catal.* **155**, 204 (1995).
31. Butler, J. D., and Davis, D. R., *J. Chem. Soc., Dalton Trans.* 2249 (1976).
32. Xi, G., Bao, J., Shao, S., and Li, S., *J. Vac. Sci. Technol. A* **10**, 2351 (1992).
33. Graham, G. W., Logan, A. D., and Shelef, M., *J. Phys. Chem.* **97**, 5445 (1993).
34. Belton, D. N., DiMaggio, C. L., Schmieg, S. J., and Ng, K. Y. S., *J. Catal.* **157**, 559 (1995).
35. Permana, H., Ng, S. K. Y., Peden, C. H. F., Schmeig, S. J., Lambert, D. K., and Belton, D. N., *J. Catal.* **164**, 194 (1996).
36. Ng, S. K. Y., Belton, D. N., Schmeig, S. J., and Fisher, G. B., *J. Catal.* **146**, 394 (1994).
37. Schmick, H.-D., and Wassmuth, H.-W., *Surf. Sci.* **123**, 471 (1982).
38. Alvero, R., Bernal, A., Carrizosa, I., and Odriozola, J. A., *Inorg. Chim. Acta* **140**, 45 (1987).

39. Novak, E., and Solymosi, F., *J. Catal.* **125**, 112 (1990).
40. Hecker, W. C., and Bell, A. T., *J. Catal.* **85**, 389 (1984).
41. Uner, D. O., *J. Catal.* **178**, 382 (1998).
42. Daniel, W. M., Kim, Y., Peebles, H. C., and White, J. M., *Surf. Sci.* **111**, 189 (1981).
43. Habraken, F. H. P. M., Hieffer, E. Ph., and Bootsma, G. A., *Surf. Sci.* **83**, 45 (1979).
44. Hoffman, D. A., and Hudson, J. B., *Surf. Sci.* **180**, 77 (1987).
45. Cunningham, J., Hickey, J. N., Cataluna, R., Conesa, J.-C., Soria, J., and Martinez-Arias, A., *in* "Proceedings, 11th Internation Congress on Catalysis—40th Anniversary, Baltimore, 1996" (J. W. Hightower, W. N. Delgas, E. Iglesia, and A. T. Bell, Eds.), Vol. 101, p. 681. Elsevier, Amsterdam, 1996.
46. Isa, S. A., and Saleh, J. M., *J. Phys. Chem*. **76**, 2530 (1972).
47. Li, Y., and Armor, J. N., *Appl. Catal. B* **1**, L21 (1992).
48. Redmond, J. P., *J. Catal.* **7**, 297 (1967).